Journal of Materials Science and Engineering with Advanced Technology
Volume 5, Number 2, 2012, Pages 135-151

STRUCTURAL, TRANSPORT PROPERTIES AND DIFFUSION STUDY OF OXYGEN ATOMS FOR Mn_2-W TYPE HEXAFERRITE DOPED WITH Cu^{2+}

M. EL-SAADAWY

Department of Physics
Faculty of Science
Kafrelsheikh University
Kafrelsheikh City
Egypt
e-mail: elsaadawy2000@yahoo.com

Abstract

Series of polycrystalline samples of $Mn_{2-x}Cu_x Ba Fe_{16}O_{27}$ were prepared by usual ceramic methods, where x = 0.0, 0.4, 0.6, 0.8, 1.0, 1.2, 1.4, and 1.6. X-ray analysis were obtained at room temperature by using Cok_α with confirms the presence of W-type hexaferrite phase structure. The dc electrical conductivity (σ_{dc}) and the dielectric constant (ε) were studied. The experimental results showed that dc resistivity, dielectric constant, Curie temperature, and activation energies for electrical conduction increase as Cu ion substitution increases. The dc electrical conductivity increases as temperature increases. The oxygen diffusion in the samples at annealing temperature of 850°C for 1 min, was studied. The diffusion coefficient was calculated by using the equation $D = \left(\frac{\sigma_{dc} k_B T}{Ne^2}\right) t$. It was found that the oxygen diffusion is characterized by a relatively small activation energy (0.215eV) and low pre-exponential factors

Keywords and phrases: X-ray analysis, electrical properties, charge carrier concentration, diffusion coefficient, Mn_2-W hexagonal ferrite.

Received February 25, 2012

$D_0 \approx 5.55 \times 10^{-13} \mathrm{m}^2.\mathrm{sec}^{-1}$. The substitution of Cu ions decreases the diffusion coefficient up to $x = 1.2$ and then increase it.

1. Introduction

Today ceramic magnetic materials, capable of combining a high resistivity and a high permeability, are found in numerous products used in our every day life, such as home appliances, electronic devices, communication equipments, and computers [12]. Polycrystalline ferrites are good magnetic semiconductors with low electrical conductivity and low eddy currents. They play an important role in various technological applications from microwave to radio wave frequencies. In particular, the specific magnetic moment can be greatly increased by the presence of divalent or trivalent nonmagnetic ions in the tetrahedral sites of which, there are a relatively large number in this structure. W-type hexagonal ferrite has the chemical formula $BaMe_2Fe_{16}O_{27}$ and its composition consists of one molecular unit M-type hexagonal ferrite having chemical formula $BaFe_{12}O_{19}$ and two unit spinel ferrite having chemical formula, i.e., $W = M + 2S\,(Me_2W$, Me = Mn, Cu, Co, Zn, etc.) have a crystalline structure built up as a stacking of R and S blocks along the hexagonal c axis, RSR^*S^* for M type, where R is a three oxygen-layer block with composition $Ba\,Fe_6\,O_{11}$, S (spinel block) is a two-oxygen-layer block with composition $Fe_6\,O_8$, and the asterisk means that the corresponding block has been rotated by 180° around the hexagonal c axis. Both the distribution and the spin orientation of the cations for the various sub lattices of W-type hexagonal ferrite are listed in [13]. Due to these reasons, the W-hexaferrites appear as promising materials for technological application in the fields of permanent magnets and microwave devices. Recently, the surface mounting devices have been rapidly developed for electronic application, such as multilayer chip beads or inductors. They are important components for the latest products, such as cellular phones, video cameras, and notebook computers, hard and floppy drives. Polycrystalline ferrites have been used widely because of

their high permeability in the RF frequency region, high electrical resistivity, and environmental stability [8]. In 1976, one reported for the first time the magnetic properties and Mossbauer spectrum of Zn_2-W hexaferrite [10]. Thermal conductivity and thermoelectric power studies of some cobalt substituted BaZnW-type hexagonal ferrites were undertaken as a function of composition and temperature [2]. Magnetic properties of $Mg_xZn_{1-x}2W$ and $Mn_xZn_{1-x}2W$ ferrites were studied [1]. DC conductivity for hexaferrites of $Zn_{2-x}Cu_x\ Ba_1Fe_{16}O_{27}$ system were studied [3]. The lack of information about the oxygen diffusion in ferrite has been the main reason for introducing these investigations. In addition, the diffusion information may be helpful in analyzing the structural defects in the oxygen sublattice. This work on the diffusion may reinforce the existing concept that the diffusion of cation vacancies is faster than that of anions . These and other factors relating to the oxygen diffusion are important for understanding the process, which takes place during the ferrite synthesis (thermal and thermomagnetic treatment and operations of ferrites).

2. Results and Discussion

2.1. X-ray diffraction of $Mn_{2-x}Cu_xBaFe_{16}O_{27}$

The diffraction patterns of the samples, where x = 0.0, 0.4, 0.6, 0.8, 1.0, 1.2, 1.4, and 1.6 were obtained at room temperature by using Cok_α with $\lambda = 1.7902A^o$. Figures 1(a) and 1(b) show the X-ray diffraction pattern for the mentioned compositions. The diffraction patterns confirm the presence of W-type hexaferrite phase structure. The measured values of *d*-spacing and the corresponding miller indices for each pattern are tabulated in Table 1.

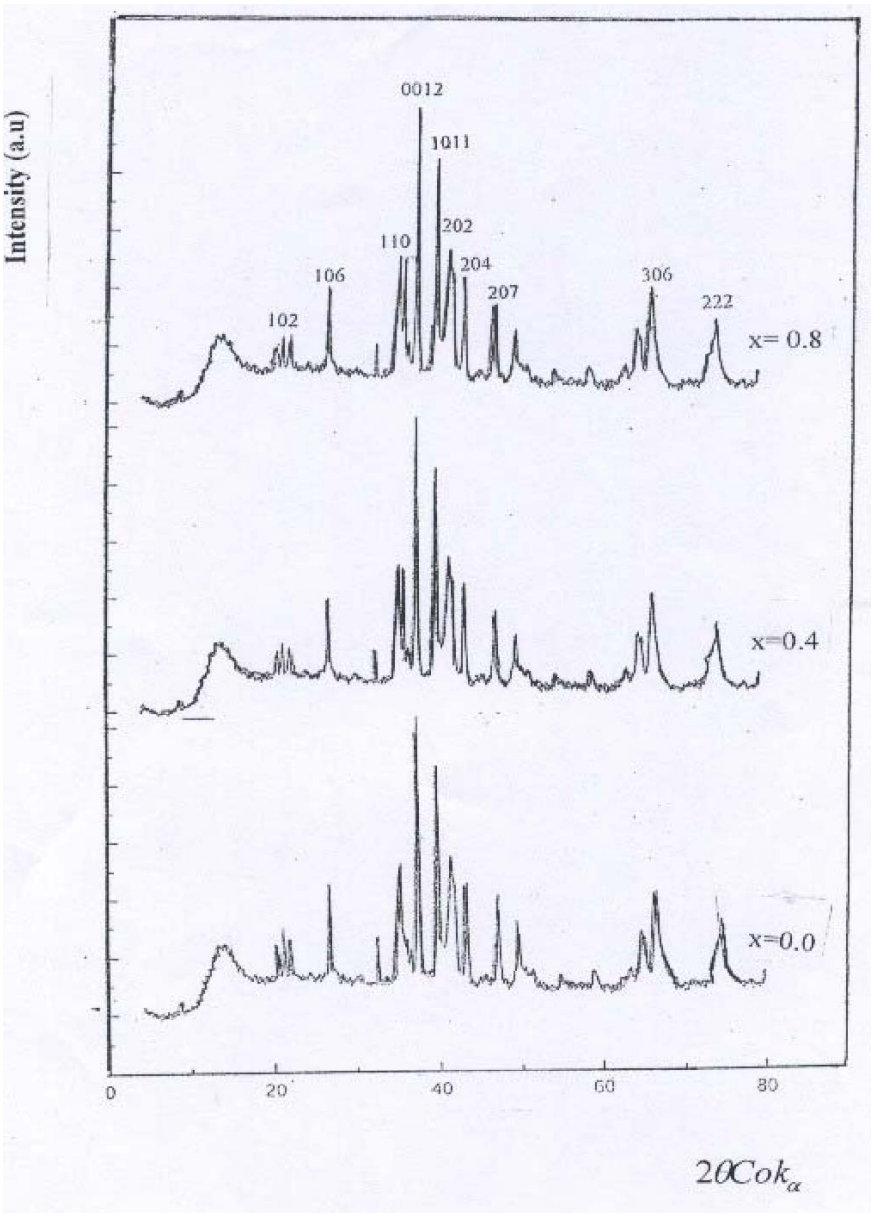

Figure 1(a). X-ray diffraction pattern of $Mn_{2-x}Cu_xBa\ Fe_{16}O_{27}$ hexagonal ferrite at room temperature (x = 0.0, 0.4, 0.8).

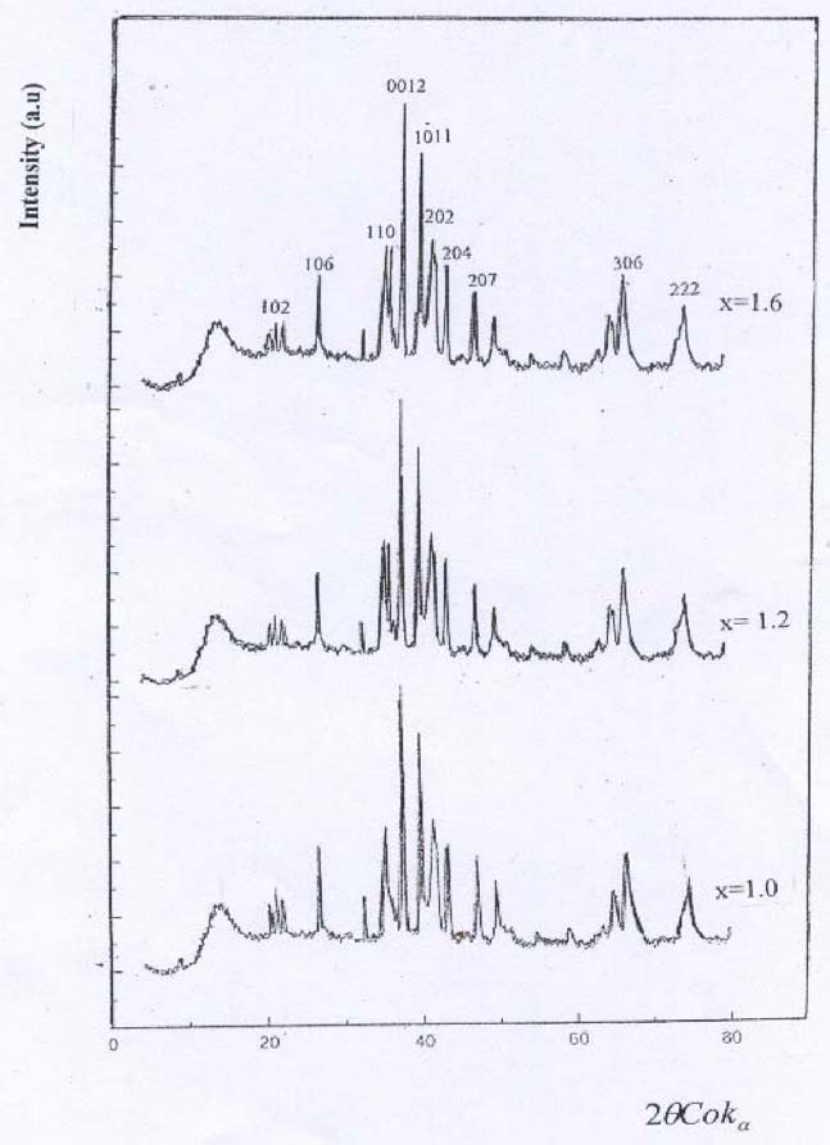

Figure 1(b). X-ray diffraction pattern for the samples (x = 1.0, 1.2, 1.6), which indicates tetragonal phase at (2θ = 22.06, 33.23, 36.42, 39.46, and 42.23).

Table 1. The measured values of d-spacing and the corresponding miller indices for each pattern for the sample ($x = 0.0$, $x = 0.6$)

$x = 0.0$			$x = 0.6$		
2	d	hkl	2	d	hkl
20.86	4.94	102	20.86	4.86	102
22.30	4.628	103	22.30	4.62	008
26.80	3.862	106	26.80	3.85	106
32.53	3.196	0010	32.53	3.23	110
35.60	2.93	110	35.60	3.11	112
36.21	2.88	112	36.21	2.82	0012
37.73	2.768	1010	37.73	2.52	204
38.87	2.69	0012	38.87	2.53	207
38.87	2.61	1011	38.87	2.32	1014
41.60	2.52	202	41.60	1.92	216
47.55	2.22	207	47.55	1.66	2015
50	2.118	1014	50	1.56	306
54.83	1.944	2012	54.83	1.45	3010
58.92	1.82	216	58.92	1.22	2012
63.51	1.7	300	63.51	1.01	216
63.51	1.66	304	63.51	0.87	300
67.31	1.61	2016	67.31	0.83	304
75.29	1.46	222	75.29	0.75	2016

The lattice parameters were calculated from the relation [9]

$$\frac{1}{d^2_{hkl}} = \frac{4b^2 + hk + k^2}{3a^2} + \frac{l^2}{c^2}, \tag{1}$$

where d_{hkl} is interplanar distance. The variation of lattice parameter a, c, ratio c/a and porosity versus Cu substitution are tabulated in Table 2. It is shown that c, a and their ratio c/a are nearly constant with increasing Cu content and porosity is slightly increases.

Table 2. The variation of lattice parameter a, c, ratio c/a and porosity versus Cu substitution

x	a(A°)	c(A°)	c/a	P
0.0	5.842	33.42	6.166	0.10
0.4	5.836	33.56	5.750	0.14
0.6	5.872	33.27	5.666	0.17
0.8	5.846	33.53	5.736	0.20
1.0	5.861	33.45	5.707	0.21
1.2	5.880	33.42	5.683	0.22
1.4	5.902	33.58	5.689	0.24
1.6	5.931	33.64	5.642	0.27

This behaviour can be explained on the basis of ionic radii of substituted ions, where the ionic radius of substituted Cu^{2+} ions is 0.96A°, which is nearly of the same order of that of Mn^{2+} ions 0.80A°. This confirms that Cu^{2+} ion replace Mn^{2+} ion in the structure. The value of the lattice parameters for our structure are a = 5.84nm and c = 33.4nm. The X-ray diffraction patterns indicates the presence of tetragonal phase due to the Jahn-Teller effect of the Cu^{2+} ions located at octahedral B sites. There are some peaks appeared in the patterns corresponds to the sample with Cu^{2+} ion and belongs to tetragonal phase. These peaks appeared at 2θ = 22.06, 33.23, 36.42, 39.46, and 42.23 with corresponding d values equals to 4.76, 3.23, 2.65, and 2.45nm. For the hexagonal structure, the X-ray density is calculated according to the relation

$$D_x = \frac{2M}{NV}, \tag{2}$$

where V is the volume of the unit cell $V = a^2 c \sin 120$, M is the molecular weight, and N is Avogadro's number. The porosity P was calculated for each sample from the relation

$$P = 1 - \frac{D}{D_x}. \tag{3}$$

The experimental density D and porosity P, were calculated for each composition.

Figure 2 shows the variation of the experimental density D, X-ray density D_x as a function of copper content (x). It is shown that the experimental density is slightly decreases with copper content. The X-ray density is about 5.742gm/cm^3.

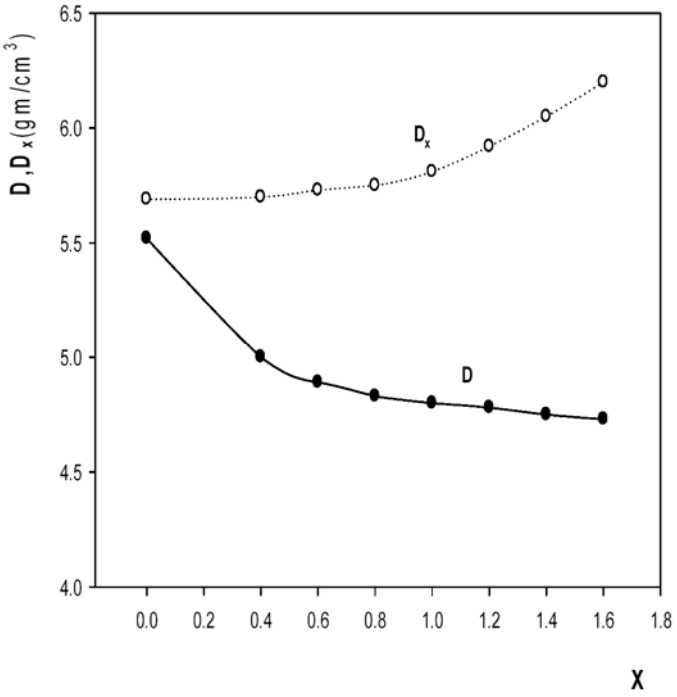

Figure 2. The variation bulk density, X-ray density as a function of copper content (x).

2.2. Temperature dependence of the electrical conductivity (σ_{dc})

The relationship between the calculated values of the $Ln\sigma_{dc}$ and the $10^3 / T$ is illustrated in Figure 3. It is clear that the dc electrical

conductivity increases as the temperature increases. This is the normal behaviour of semiconductors, which is controlled by the verifying the Arhenius equation

$$\sigma_{dc} = \sigma_0 \exp\left(\frac{-Eg}{k_B T}\right), \tag{4}$$

where σ_0 is a constant, E_g is activation energy for electrical conduction, and k_B is the Boltzmann's constant. The conductivity σ_{dc} is what we determine from measuring the resistivity ρ_{dc} of the samples at different temperature, along with the formula

$$\sigma_{dc}(T) = \frac{1}{\rho_{dc}(T)} = \frac{d}{R.S}(\Omega^{-1}\mathrm{cm}^{-1}), \tag{5}$$

where R, S, and d are resistance of the sample in Ohm, the sample area in cm^2, and the sample thickness in cm, respectively, and $\rho_{dc}(T)$ is the resistivity of the sample and temperature dependent. The transition temperature from ferrimagnetic to paramagnetic corresponds to a break in line, which represents the relation between $Ln(\sigma_{dc})$ and $10^3/T$. This breaks also corresponds to the transition from tetrahedral spinel structure to spinel cubic structure. These results are in agreement with preview work [3, 4]. At this temperature, small abrupt rises in conductivity is formed. This transition is first order phase transition [11]. The structural phase transition occurs at a temperature slightly below Curie temperature, due to the cooperative Janhn-Teller effect.

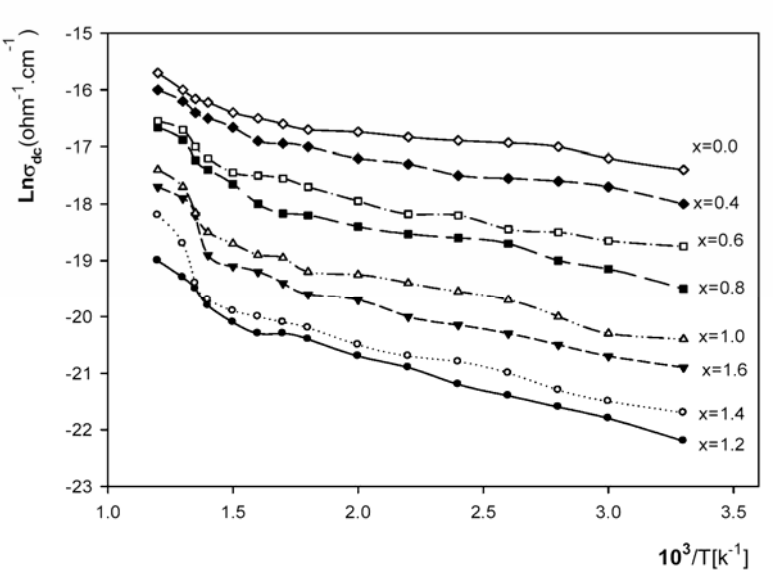

Figure 3. The *Ln dc* conductivity $(Ln\sigma_{dc})$ of studied samples as a function of $10^3/T$ system.

2.3. Effect of temperature and frequency on the dielectric constant

The variation of the dielectric constant (ε) with temperature at 100kHz for $Mn_{2-x}Cu_xBa\ Fe_{16}O_{27}$ (x = 0.0, 0.4, 0.6, 0.8, 1.0, 1.2, 1.4, and 1.6) is shown in Figure 4. It can be seen from the figure that the dielectric constant increases with temperature, as expected for the semiconducting behaviour. This is attributed to the following: The substitution of Cu ion into Mn-W type hexaferrite might cause the formation of excess vacancies. Also, lattice vacancies are created by substitution of impurities with incorrect vacancies and by changes in stoichiometry [7]. So, charged oxygen vacancies are introduced when Cu^{2+} replaces Fe^{3+}. These vacancies are believed to be absorbed at grain boundaries retarding charge mobility and causing an increase in polarization. The substitution of Cu^{2+} ions for the Mn^{2+} ions at the A sites caused these ions to

migrate to the octahedral configuration. The electric exchange gives local displacement of electrons in the directions of an applied electric field, which induces polarization in ferrites. The increase of the hopping electrons between Fe^{2+} and Fe^{3+} in the direction of the applied field with rising temperature and also the increase of the hopping holes between Cu^{2+} and Cu^{3+} at B sites lead to an increase in polarization at the sample surface and hence the dielectric constant. Figure 5 represents the frequency dependence of the dielectric constant at room temperature for different compositions. It can be obviously notice that the sample of x = 1.0 (high value Cu content) shows higher frequency dependence at room temperature besides it has a relatively high value of (ε) [14]. In other words, by increasing Cu content, the dielectric constant increases.

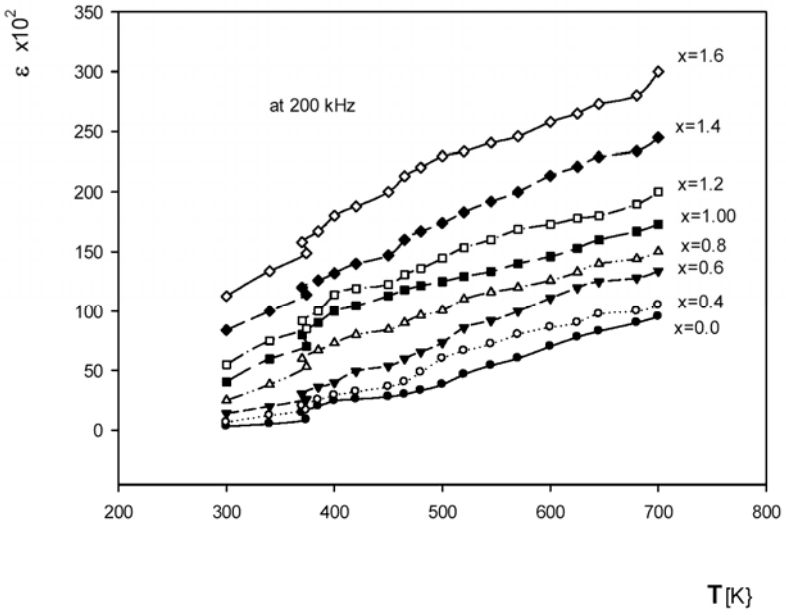

Figure 4. Variation of the dielectric constant with temperature at 200kHz for the studied samples.

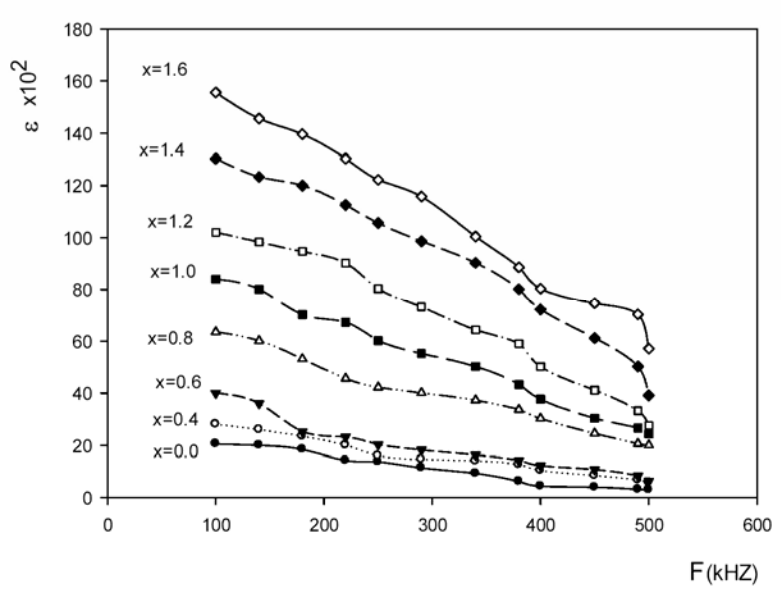

Figure 5. Frequency dependence of the dielectric constant at room temperature for studied samples.

2.4. Effect of temperature on the oxygen diffusion coefficient

The diffusion coefficient of oxygen vacancies $(Ln(D))$ in $Mn_{2-x}Cu_x$ $Ba_1Fe_{16}O_{27}$ hexagonal ferrite (x = 0.0, 0.4, 0.6, 0.8, 1.0, 1.2, 1.4, and 1.6) as a function of $10^3/T$ is illustrated in Figure 6. The diffusion coefficient of oxygen vacancies is estimated from the relation [6]: $\sigma_{dc} = \left(\frac{Ne^2D}{k_BT}\right)t$, where σ_{dc} is the dc electrical conductivity, N is the number of atoms $m^{-3} = 4\times10^{22}$, e is the electronic charge, and t is the annealing time in sec. A noticeable increase of diffusion coefficient (D) with increasing temperature occurred. The oxygen vacancies have been reported to accelerated densification during sintering process. The diffusion of oxygen ions can usually only occur, however, if defect or structural vacancies are present in the structure, because otherwise, there is no possibility of an anion jumping into a neighbouring lattice site. In our composition, Cu^{2+}

leading to migration very small ratio Mn ions to replace Fe^{3+} at octahedral sites. The substations of Mn^{2+} instead of Fe^{3+} create lattice vacancies, since the vacancy of Mn^{2+} ions is less than that of Fe^{3+} ions, which may cause high diffusion rate through the grain boundaries tending to increase the conductivity with a maximum value at $x = 1.2$, and then decrease for higher concentration. The increase of temperature increases the mobility of vacancies, which help more oxygen vacancies to be diffused. From Figure 6, we can notice the effect of Cu ion substitution on the diffusion of oxygen vacancies in the given ferrite. The diffusion of oxygen vacancies decreases as Cu ion concentration increase up to = 1.2, and then increases for higher concentrations. This can be explained by the following: The substitution of Cu^{2+} instead of Mn^{2+} ion might cause the formation of lattice vacancies leading to the increase of diffusion of oxygen vacancies during sintering for $x \geq 1.2$. For Cu concentrations $x \leq 1.2$, the lattice vacancies are occupied by cations and the cation vacancies increased, which reduce the diffusion of oxygen vacancies during sintering. From the calculated diffusion coefficient, we notice first that the diffusion coefficient of oxygen measured by us $(D = 10^{-13} - 10^{-15} \mathrm{m}^2\mathrm{sec}^{-1})$ is the higher range with that studied in [5, 6], which were measured at similar temperature intervals. The high values of the oxygen diffusion coefficient are due to large pre-exponential factor D_0 in the temperature dependence $D_0 = D_0 \exp\left[\frac{-E}{k_B T}\right]$. The D_0 for every sample is given in Table 3, where it is given in the previous work [5] on Ni ferrite $Ni_{0.8}Fe_{2.2}O_4$ as $D_0 = 4.68 \times 10^{-15} \mathrm{m}^2\ \mathrm{sec}^{-1}$.

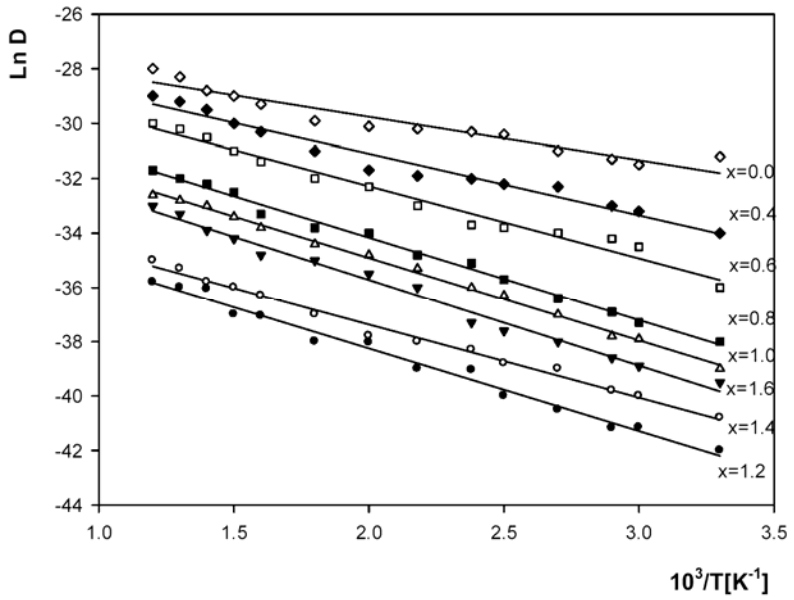

Figure 6. The *Ln* diffusion coefficient of oxygen of oxygen atom in the studied samples as a function of $10^3/T$.

Table 3. Variation of diffusion coefficient of oxygen vacancies (LnD), pre-exponential factor (D_0), and concentration of structural vacancies (n_ν) versus Cu substitution

X	LnD	$D_0 x10^{-13}\left(\mathrm{m}^2.\sec^{-1}\right)$	$n_\nu x10^{-3}(\mathrm{m}^{-3})$
0.0	– 28.22	5.5489	5.549
0.4	– 28.66	3.5737	3.574
0.6	– 29.50	1.5428	1.5428
0.8	– 30.44	0.60266	0.60266
1.0	– 31.50	0.20874	0.2088
1.2	– 34.80	0.0078	0.0077
1.4	– 33.50	0.028257	0.02826
1.6	– 32.20	0.10368	0.1037

One more important conclusion may be drawn from the analysis of D_0 and the activation energy (E) determined in this study that in our samples, the oxygen atoms diffuse through structural vacancies rather than thermal equilibrium vacancies in the oxygen sublattice. This inference is supported first by a low diffusion activation energy (e = 0.215eV). When thermal equilibrium vacancies are involved in diffusion, the diffusion activation energy is equal to the sum of the oxygen atom migrating energy (E_m) and the vacancy formation energy (E_f), i.e., $E = E_m + E_f$. Moreover, E_f usually exceeds 1eV. The oxygen vacancies activation energies for the given ferrites are shown in Figure 7. It seems to be increased with increasing Cu ion concentrations up to $x \leq 1.2$ and then decreased for $x = 1.6$. The increase of Cu ions creates more lattice vacancies, which increase the diffusion process and decrease the activation energy of diffusion. On the other hand, if diffusion involves structural vacancies, the order of D_0 is roughly determined by the following expression [5]: $D_0 = a^2 \nu n$, where $a \cong 10^{-10}$m is lattice constant, $\nu \cong 10^{12}\text{sec}^{-1}$ is the vibration frequency of oxygen atoms in the lattice, n_ν is the concentration of structural vacancies. Taking into account, the value of D_0 the order of the concentration of structural vacancies may be estimated at about $5.5 \times 10^{-5} - 77 \times 10^{-9}$ as given in Table 3, and it seems to be higher than the data given in the previous work [5, 6], which was in the range of $10^{-9} - 10^{-11}, 10^{-13} - 10^{-12}$. Therefore, these results may be treated as a serious attempt to measure the concentration of structural vacancies in the compounds, which can hardly be measured by other techniques. The difference between our present values of D_0 and the previous values is the doping of cation sublattice with impurities. A very low value of the activation energy (0.215eV) and the corresponding higher mobility of structural oxygen vacancies indicate that oxygen vacancies may participate in the local

rearrangement of the structure during the sintering process that determines the thermomagnetic properties ferrite.

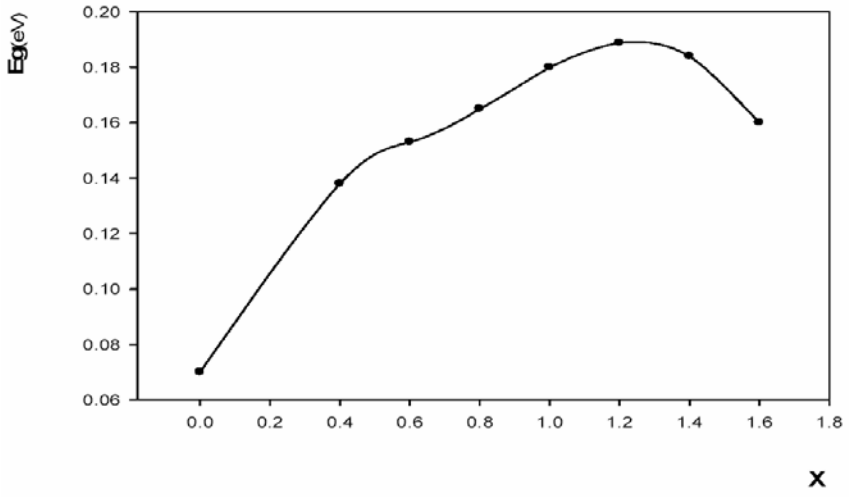

Figure 7. The activation energy of the diffusion of oxygen vacancies in the given ferrite at room temperature.

References

[1] T. Aoyama, K. Hirota and O. Yomaguchi, Characterization and low-temperature sintering of reactive Mn-Zn ferrite powder, J. Am. Ceram. Soc. 79 (1996), 2792-2794.

[2] M. El-Saadawy, Thermal conductivity and thermoelectric power of the $Zn_{2-x}Co_xBaFe_{16}O_{27}$ hexagonal ferrites system, J. Materials Letters 39 (1999), 149-152.

[3] M. El-Saadawy, DC conductivity for hexaferrites of the $Zn_{2-x}Cu_xBaFe_{16}O_{27}$ system, J. Magn. Magn. Mater. 219 (2000), 69-72.

[4] M. El-Saadawy, Electrical properties of $Co_{2-x}Zn_xBa_2Fe_{28}O_{46}$ hexagonal ferrite, J. International Ceramic Review (2003), 206-210.

[5] M. El-Saadawy, The diffusion coefficient of vacancies and jump length of electrons in nickel doped magnesium ferrite, Oriental Journal of Physics 1 (2009), 9-16.

[6] O. M. Hemeda, M. El-Saadawy and M. M. Barakat, The diffusion study of oxygen atoms in $Co_{x/3}Ni_{(5-x)/3}Sb_{1/3}Fe_1O_4$ ferrite, J. Magn. Magn. Mater. 219 (2000), 73-77.

[7] A. Kumar and S. Sharma, Measurement of dielectric constant and loss factor of the dielectric material at microwave frequencies, Progress in Electromagnetic Research, PIER 69 (2007), 47-54.

[8] H. Montiel, G. Alvarez, M. P. Gutiérrez, R. Zamorano and R. Valenzuela, Microwave absorption in Ni-Zn ferrites through the Curie transition, J. Alloys and Compound 369 (2004), 141-143.

[9] M. Z. Said, D. M. Hemeda, S. Abdel Kader and G. Z. Farag, Structural, electrical and infrared studies of $Ni_{0.7}CD_{0.3}SM_xFe_{2-x}O_4$ ferrite, Oriental Journal of Physics 1 (2009), 17-29.

[10] D. Samaras, The rotation of the magnetization in the $BaCo_2Fe_{16}O_{27}$ W-type hexagonal ferrite, J. Magn. Magn. Mater. 79 (1989), 193-197.

[11] E. E. Sileo, R. Rotelo and S. E. Jacobo, Nickel-zinc ferrites prepared by the citrate precursor method, Physica B: Condensed Matter 320 (2002), 257-260.

[12] D. Stoppls, Developments in soft magnetic powder ferrites, J. Magn. Magn. Mater. 160 (1996), 323-328.

[13] B. Viswanathan and V. R. K. Murthy, Ferrite Materials: Science and Technology, Narosa Publishing House, New Delhi, (1990), 429-434.

[14] W. R. Wang, S. F. Wang and Y. M. Lin, Low temperature sintering of $(Zn_{1-x}Mg_x)TiO_3$ microwave dielectric, Ceramic International 31 (2005), 905-909.

■